

Supporting Information

Hydrocarbon-based Pemion™ proton exchange membrane fuel cells with state-of-the-art performance

Hien Nguyen^{1,2}, Florian Lombeck², Claudia Schwarz², Philipp A. Heizmann¹, Michael Adamski³, Hsu-Feng Lee³, Benjamin Britton³, Steven Holdcroft⁴, Severin Vierrath^{1,2} and Matthias Breitwieser^{1,2}

1. Electrochemical Energy Systems, IMTEK - Department of Microsystems Engineering, University of Freiburg, Georges-Koehler-Allee 103, 79110 Freiburg, Germany
2. Hahn-Schickard, Georges-Koehler-Allee 103, 79110 Freiburg, Germany
3. Ionomr Innovations Inc., 111-2386 East Mall, Vancouver, BC V6T 1Z3, Canada
4. Department of Chemistry, Simon Fraser University, Burnaby, BC V5A 1S6, Canada

Optimization of I/C Ratio for Pemion™-based and PFSA reference MEA

Figure S1 shows the performance of Pemion™-based MEA and PFSA reference with increasing I/C ratio, starting from I/C = 0.2, in standard H₂/O₂ operations (0.25 slpm/1 slpm gas feed, 95 % RH and ambient pressure). The results show that the performance of the Pemion™-based MEA with I/C = 0.2 is enhanced over I/C = 0.4 while that of PFSA reference is enhanced with higher ionomer content (I/C = 0.4).

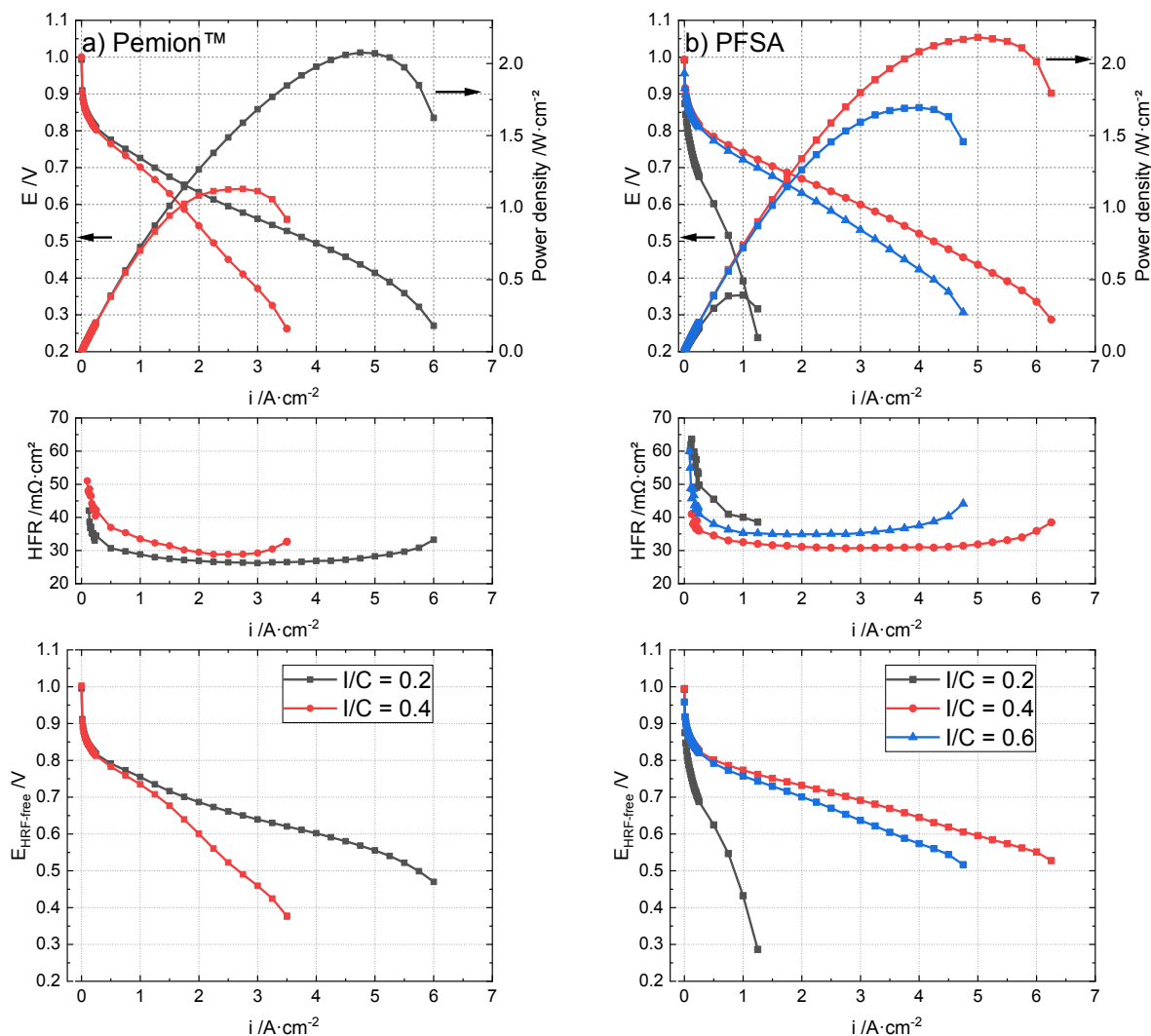


Figure S1: Polarization behaviours, HFRs and HFR-corrected cell voltages of (a) Pemion™ MEA vs. (b) PFSA reference with varied I/C ratios in H_2/O_2 , 0.25/1 slpm gas feed, 95 % RH and ambient pressure.

Proton conductivity measurements

The proton conduction resistance of the cathode, $R_{H^+,cath}$ (in units of $m\Omega \cdot cm^2$), is determined from AC impedance spectra recorded in H_2/N_2 (anode/cathode) at 0.2 V with a peak-to-peak perturbation of 1.75 mV between 100 kHz and 0.2 Hz (20 points per decade). To ensure reproducibility, each measurement is repeated three times. The resulting experimental data is evaluated following the approach proposed by Lefebvre *et al.*¹, Touhami *et al.*² The ionic resistance in the CL, R_{H^+} , can be estimated from the profile of the Nyquist plots: the intersection between the tangent of the length of the “low-frequency line” or the “Warburg-like region” and the real impedance $Re(Z)$ axis is $R_{H^+}/3 + R_{HFR}$. Representative measurement data (dots) with the corresponding fits for the low-frequency line ($\omega \rightarrow 0$) are shown in Figure S2.

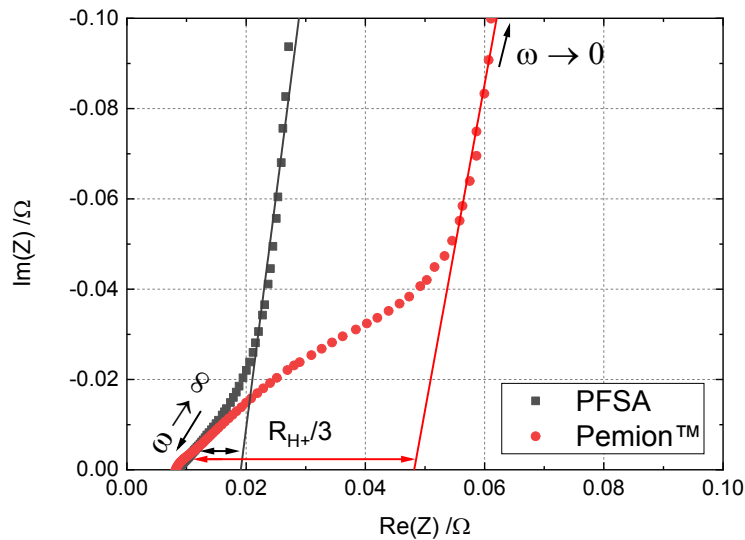


Figure S2: Protonic impedance of cathode CLs containing Pemion™ and PFSA ionomer obtained under H_2/N_2 (0.5 slpm/0.5 slpm) at 80 °C, 95 % RH and ambient pressure.

Tafel slopes

Figure S3 shows the Tafel slope of both MEAs extracted between 25 $\text{mA}\cdot\text{cm}^{-2}$ and 100 $\text{mA}\cdot\text{cm}^{-2}$ from the $E_{iR\text{-free}}$ cell voltages under H_2/O_2 and log of crossover-corrected current density $i + i_x$.

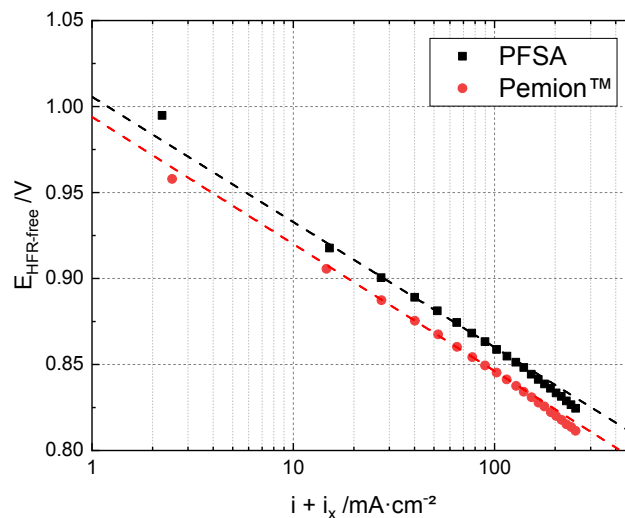


Figure S3: Tafel region corrected for Ohmic resistances as well as by the H_2 crossover current density under H_2/O_2 , 80 °C, 95 % RH, ambient pressure.

Hydrogen Adsorption/Desorption

Following the conventional approach of integration of the hydrogen adsorption current (between 0.08 V and 0.1 V) subtracting the double-layer current extrapolated from intermediate potentials (ca. at 0.4 V) and assuming 1 H^+ per surface Pt atom ($210 \mu\text{C}\cdot\text{cm}^{-2}_{\text{Pt}}$).

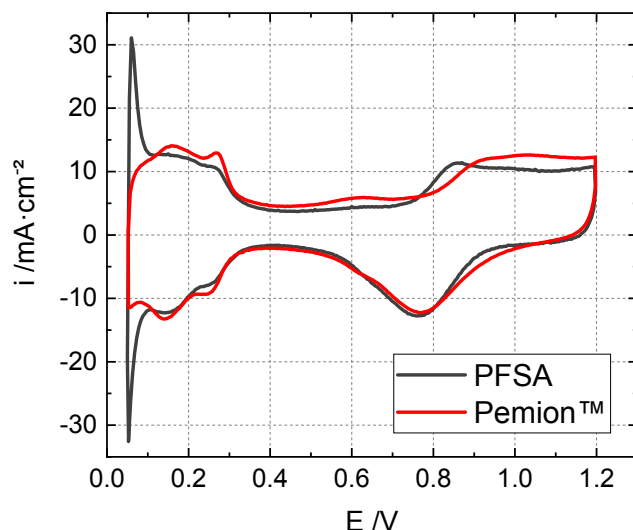


Figure S4: Cyclic voltammograms of PtCo/C with Pemion™ vs. PFSA under 35 °C, 95 % RH and 50 mV·s⁻¹ scan rate.

Despite the much lower ionomer content in dry CL of Pemion™ MEAs (9 wt %) compared to that of a PFSA reference (18 wt %), the electrochemical active surface area (ECSA) of Pemion™ MEAs (43 m²·g⁻¹) is comparable to that of PFSA MEAs (41 m²·g⁻¹). These values are similar with those of PtCo/C catalyst with PFSA determined with the H_{upd} method reported in literature^{3,4} and with those using Pt/C catalyst with sPPB-H⁺ reported by Balogun *et al.*⁵ The lower ECSAs of PtCo/C determined by H_{upd} compared to the ECSAs of Pt/C determined by H_{upd}³ or to the ECSAs of PtCo/C determined by other methods is likely due to the presence of Co surface atoms that do not participate in the H_{upd} adsorption process.⁴

Cyclic Voltammograms under Different Relative Humidities

Figure S2 presents the cyclic voltammograms of the Pemion™ and the PFSA reference MEAs acquired under increasing RH levels. The profiles of the cyclic voltammograms for both MEAs significantly change with increasing humidity operation, with Pemion™ exhibiting a larger differential than the PFSA reference.

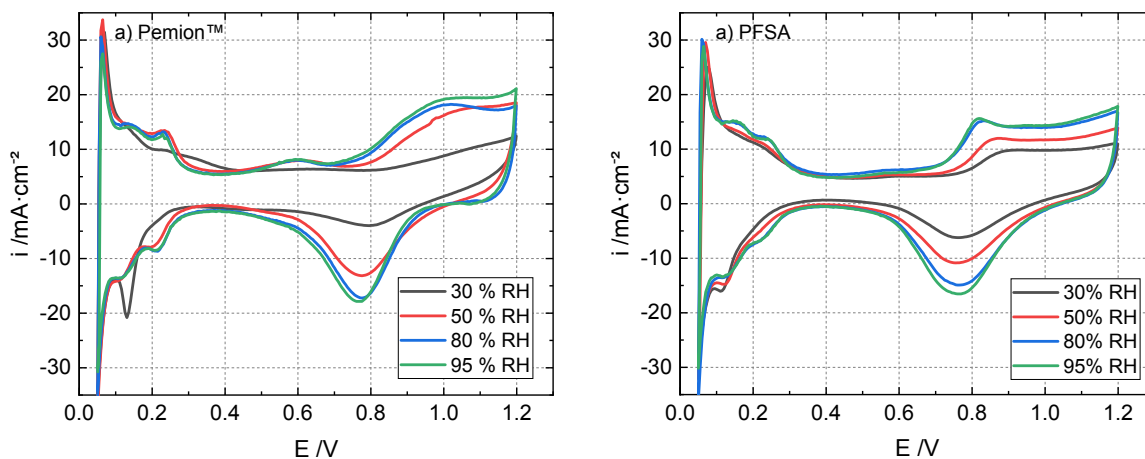


Figure S5: Cyclic voltammograms of (a) Pemion™ MEA and (b) PFSA reference at different RH levels.

At oxide formation region (at potentials ≥ 0.8 V) the typical redox reaction at Pt surface is expressed as following⁶



A high RH is associated with higher H_2O activity. Hence, higher current density maxima are obtained at higher RH. The onset potential for the adsorption and reduction of oxygenated species such as hydroxides (Pt-OH) and oxides (Pt-O) on Pt surface in PFSA (Figure 5b) is shifted to lower potentials as the RH increases. This result is in accordance to the theoretical Nernstian response of the oxidation reaction presented with Equation 1 and to the response reported in literature.^{3,7,8}

With Pemion™ as solid polymer electrolyte (Figure 5a), the potentials for the reduction of Pt surface on the cathodic scan are at around 0.8 V, which are similar to PFSA reference. On the anodic scan, two oxidation current peaks are observed at ~ 0.6 V and ~ 1.0 V, which are different from the anodic current response of PtCo in PFSA. This anodic current response is also observed in the study of Lindström *et al.*⁹ on PSUGPVPA as hydrocarbon-based solid electrolyte. These current density peaks present other oxidation processes at the Pt surface that can possibly be induced from the adsorption and oxidation of other anions such as the excessive sulfonic acid groups (SO_3^-)¹⁰ at the side-chains of the Pemion™ ionomer due to the high IEC and/or the aromatic groups in the backbone of Pemion™. Since the 1980s, several researchers such as the group of Hubbard^{11,12} or Gattrell and Kirk¹³ have been studied systems based on platinum/aromatic compounds such as hydroquinone, benzoquinone or phenol in aqueous solutions. The studies proposed chemisorption of small aromatic compounds on Pt surfaces is causal to subsequent irreversible oxidation of the particles. However, it is notable that aromatic polymers act differently than small molecules due to the high molecular weight, rigidity, and steric hindrance of polymers reducing the ability of aromatic groups to attain a preferential geometry for interaction, particularly in the Pemion™ structure, and these factors will also vary with λ -value.

It is also striking that no Pt oxidation peak can be identified in the cyclic voltammogram of Pemion™ MEA at 30 % RH (Figure 5a) and the corresponding reduction peak is less distinctive as those at higher RH. It was suggested by Gattrell and Kirk in their study with phenol/platinum system that the formation of Pt-OH species could be inhibited by the presence of a high coverage of phenol.¹³ This might be the case for Pemion™ that in low RH (here: 30 %) the -OH coverage on Pt surface is inhibited by the coverage of phenyl in Pemion™. Other characterizations on Pt(-Co)/Pemion™ system are ultimately required in future work to confirm these presumptions. The consequent ORR kinetics with Pemion™ upon humidity changes as lower RH results into lower OH-coverages remains an open question.

At hydrogen adsorption (cathodic sweep)/desorption (anodic sweep) region, i.e. at potentials between 0.05 and 0.4 V, the typical redox reaction at Pt surface is expressed as following⁶



While the dependency of the current response for Pt oxide on RH is unambiguous and well-reported in literature,^{3,6} the dependency of the hydrogen adsorption/desorption on RH is not as clear. The charge due to the hydrogen adsorption process is difficult to estimate in this case due to possible overlapping with the onset of hydrogen evolution.^{8,14} The process of hydrogen adsorption and desorption is fast and ideally, electrochemically reversible.

It can be observed in Figure 5 that at low RH (e.g., 30 % RH) the anodic and cathodic peaks of the cyclic voltammogram of Pemion™ are asymmetric indicating irreversible processes at the H_{UPD} region with Pemion™ at 30 % RH. It can also be seen that no hydrogen adsorption peak at around 0.22 V is observed for both PFSA and Pemion™. The same is observed by Lindström *et al.*⁹ for both PFSA and hydrocarbon-based systems as well as Xu *et al.*⁶ and Liu *et al.*⁷ for PFSA system. Apart from external factors such as temperature or humidity, the number and position of current density peaks in the hydrogen adsorption region depend on the electrolyte and the crystallographic faces of Pt exposed to the electrolyte.¹⁴ The absence of the hydrogen adsorption peak at 0.22 V might be related to the hypothesis that Pt active surface is blocked by hydrophobic domain of the solid electrolytes at low humidity as suggested by Lindström *et al.*⁸ and as previously mentioned for the oxide formation region. With increasing RH the peak around 0.22 V emerges for both Pemion™ and PFSA. Several studies with PFSA as solid electrolyte ionomers^{8,15} suggest to be related to the increasing interactions between the ionomer sulfonate (SO₃⁻) groups and the catalysts.

In the double layer region (at potentials around ~0.4 – 0.7 V), the charging/discharging of the electrochemical double layer are the only process occurring. The capacity C_{dl} obtained from the charging of the double layer and pseudo-capacity of the ion adsorption of the electrolyte is calculated as following¹⁴

$$C_{dl} = i/v \quad (3)$$

where v is the scan rate applied for the experiment (here: 50 mV·s⁻¹). The C_{dl} is reported to be closely related to the physical interface between ionomer and catalyst (including carbon supports).^{8,16,17} Figure 6 shows the C_{dl} extracted from the CVs of Pemion™ and PFSA MEA (Figure 5) relating to different RH. At RH levels higher than 50 %, the C_{dl} does not increase notably for either Pemion™ or PFSA. At 30 % RH the C_{dl} of both Pemion™ and PFSA decreases compared to that in higher RH. This is attributable to dehydration, *i.e.* shrinking of the ionomer to reduce the ionomer-catalyst/support interface.

Another interesting finding is that the C_{dl} of Pemion™ MEA is higher than that of PFSA even though the ionomer content of Pemion™ in both CLs is much lower than that in PFSA MEA (9 wt % vs. 18 wt % ionomer content). This could indicate a strong swelling behaviour of Pemion™. The swelling behaviour could be induced or be aggravated by the low ionomer content in the catalyst layer. Kusoglu and Weber¹⁸ suggested that for PFSA systems at a low I/C, the ionomer exhibits a “dispersion-like” behaviour which would result in increased swelling due to a lack of structure or phase separation. This type of behaviour may also occur in hydrocarbon-based ionomer thin films.

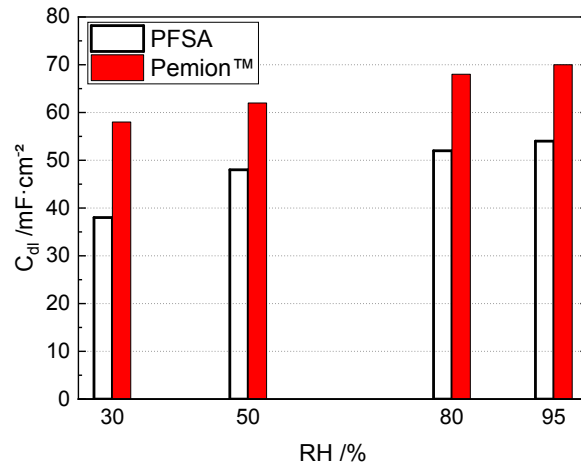


Figure S6: Double-layer capacities C_{dl} of Pemion™ MEAs and PFSA reference under varied RH levels.

Limitations other than the loss in ECSA as the RH decreases seem to contribute to a deteriorating performance at low RH for Pemion™ more significant than for PFSA. These limitations can be the increased local proton/oxygen transport resistances caused by changes of ionomer morphology at the catalyst interface due to the absence of water^{17,19,20} or changes in the ORR kinetics that may be caused by intensified interactions between the ionomer's aromatic groups and the catalyst surface, blocking the active sites of the catalyst.

Heat Rejection Limit

The rated cell voltage E_{rated} for each cell temperature T_{cell} is practically translated via the following equation,

$$\frac{Q}{\Delta T} = \frac{\text{Stack power} \cdot (1.25 - E_{rated})/E_{rated}}{T_{cell} - T_{ambient}} \quad (S1)$$

where stack power = 90 kW and $T_{ambient} = 40$ °C. The heat rejection target $\frac{Q}{\Delta T}$ is set for 2025 less than 1.45 kW·K⁻¹. The calculated cell voltages relevant for automotive applications for temperatures from 80 °C to 120 °C are presented in Table S2. The rated power density according to the DOE Target for single MEA until 2020 is over 1 W·cm⁻² at the rated cell potential.²¹

Table S1: Rated cell voltages calculated with Eq. S1 depending on the cell temperature.

Cell temperature in °C	Rated cell voltage in V
80	0.76
94	0.67
100	0.64
110	0.59
120	0.55

Further characterization of Pemion™ MEA

The cross-section Pemion™ MEA was prepared with cryo-cutting. The cross-sections of Pemion™ MEAs and the morphology of cathode CLs was characterized by scanning electron microscopy (SEM). SEM

images were acquired using a field-free SEM Amber X (TESCAN) equipped with a secondary electron in-lens and an Everhart-Thornley detector. All images were taken with an acceleration voltage of 2 keV and a beam current of 100 pA in the UH-resolution mode. The working distance was, if not mentioned otherwise, 6 mm. Figure S7 shows that the Pemion™ has a nominal thickness of $\sim 7 \mu\text{m}$.

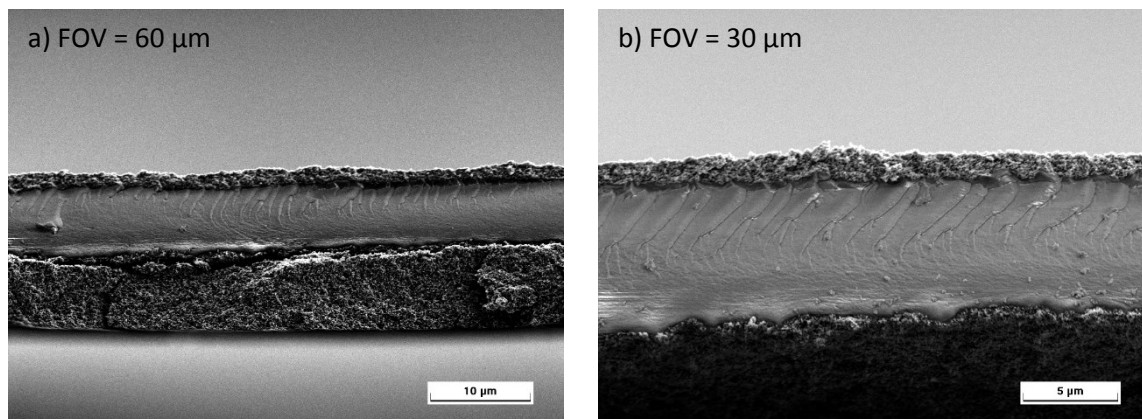
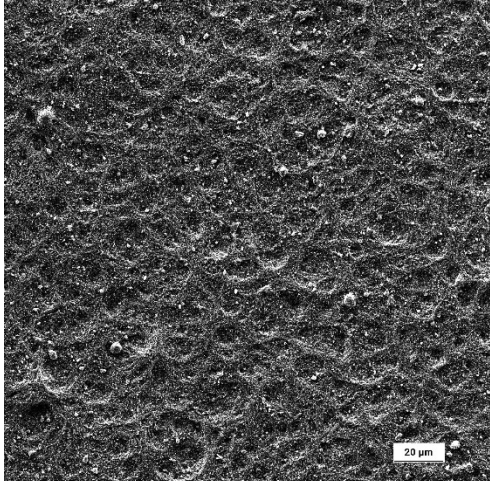
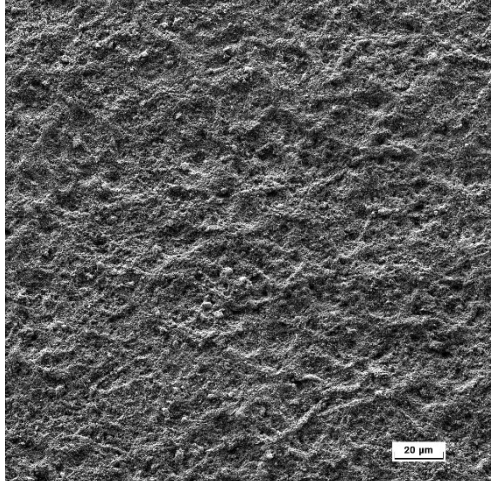
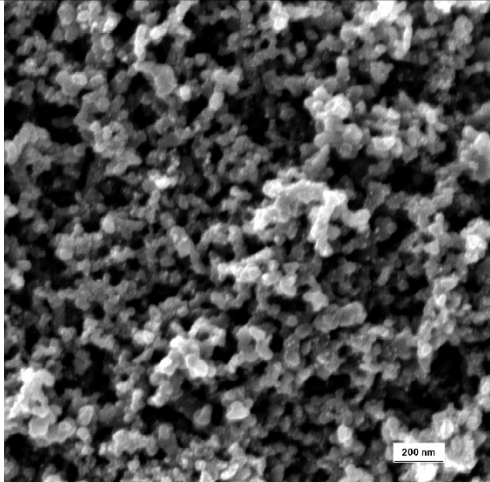
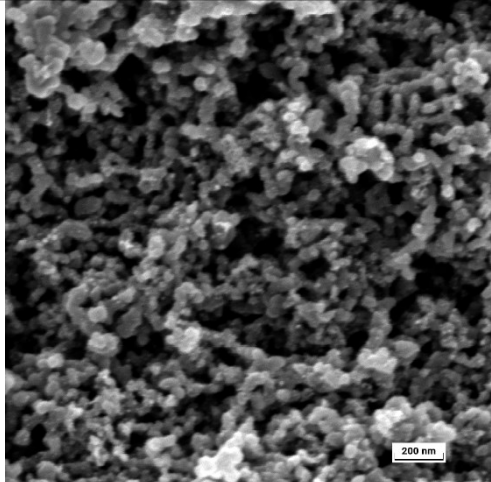


Figure S7: Cryo-cut cross-sectional morphology of Pemion™ MEA in field of views of a) 60 μm and b) 30 μm .

The morphology of the Pemion™ CL and the PFSA are alike at a 200 μm as well as at a 2 μm field of view (FoV).

MEA FoV	Pemion™	PFSA reference
200 μm	 Scanning electron micrograph (SEM) showing the morphology of Pemion™ CL at a 200 μm field of view. The surface appears as a dense, interconnected network of fine fibers or filaments. A scale bar in the bottom right corner indicates 20 μm.	 Scanning electron micrograph (SEM) showing the morphology of a PFSA reference at a 200 μm field of view. The surface morphology is very similar to the Pemion™ CL, showing a dense, interconnected network of fine fibers. A scale bar in the bottom right corner indicates 20 μm.
2 μm	 Scanning electron micrograph (SEM) showing the morphology of Pemion™ CL at a 2 μm field of view. The image reveals a porous, granular structure with irregular, interconnected particles. A scale bar in the bottom right corner indicates 200 nm.	 Scanning electron micrograph (SEM) showing the morphology of a PFSA reference at a 2 μm field of view. The morphology is highly similar to the Pemion™ CL, showing a porous, granular structure with irregular, interconnected particles. A scale bar in the bottom right corner indicates 200 nm.

References

- (1) Lefebvre, M. C. Characterization of Ionic Conductivity Profiles within Proton Exchange Membrane Fuel Cell Gas Diffusion Electrodes by Impedance Spectroscopy. *Electrochem. Solid-State Lett.* **1999**, *2*, 259.
- (2) Touhami, S.; Mainka, J.; Dillet, J.; Taleb, S. A. H.; Lottin, O. Transmission Line Impedance Models Considering Oxygen Transport Limitations in Polymer Electrolyte Membrane Fuel Cells. *J. Electrochem. Soc.* **2019**, *166*, F1209-F1217.
- (3) Wagner, F. T.; Gasteiger, H. A.; Makharia, R.; Neyerlin, K. C.; Thompson, E. L.; Yan, S. G. Catalyst Development Needs and Pathways for Automotive PEM Fuel Cells. *ECS Trans.* **2006**, *3*, 19–29.
- (4) Schulenburg, H.; Durst, J.; Müller, E.; Wokaun, A.; Scherer, G. G. Real surface area measurements of Pt₃Co/C catalysts. *Journal of Electroanalytical Chemistry* **2010**, *642*, 52–60.
- (5) Balogun, E.; Adamski, M.; Holdcroft, S. Communication—Non-Fluorous, Hydrocarbon PEMFCs, Generating > 1 W cm⁻² Power. *J. Electrochem. Soc.* **2020**, *167*, 84502.
- (6) Xu, H.; Kunz, R.; Fenton, J. M. Investigation of Platinum Oxidation in PEM Fuel Cells at Various Relative Humidities. *Electrochem. Solid-State Lett.* **2007**, *10*, B1.
- (7) Liu, Y.; Murphy, M. W.; Baker, D. R.; Gu, W.; Ji, C.; Jorne, J.; Gasteiger, H. A. Proton Conduction and Oxygen Reduction Kinetics in PEM Fuel Cell Cathodes: Effects of Ionomer-to-Carbon Ratio and Relative Humidity. *J. Electrochem. Soc.* **2009**, *156*, B970.
- (8) Lindström, R. W.; Kortsdottir, K.; Wesselmark, M.; Oyarce, A.; Lagergren, C.; Lindbergh, G. Active Area Determination of Porous Pt Electrodes Used in Polymer Electrolyte Fuel Cells Temperature and Humidity Effects // Active Area Determination of Porous Pt Electrodes Used in Polymer Electrolyte Fuel Cells: Temperature and Humidity Effects. *J. Electrochem. Soc.* **2010**, *157*, B1795.
- (9) Lindström, R. W.; Oyarce, A.; Aguinaga, L. G.; Ubeda, D.; Ingratta, M.; Jannasch, P.; Lindbergh, G. Performance of Phosphonated Hydrocarbon Ionomer in the Fuel Cell Cathode Catalyst Layer. *J. Electrochem. Soc.* **2013**, *160*, F269-F277.
- (10) Teliska, M.; Murthi, V. S.; Mukerjee, S.; Ramaker, D. E. Site-Specific vs Specific Adsorption of Anions on Pt and Pt-Based Alloys. *J. Phys. Chem. C* **2007**, *111*, 9267–9274.
- (11) Frank Lu; Ghaleb N. Salaita; Laarni Laguren-Davidson; Donald A. Stern; Edna Wellner; Douglas G. Frank; Nikola Batina; Donald C. Zapien; Nicholas Walton; Arthur T. Hubbard. Characterization of hydroquinone and related compounds adsorbed at Pt(111) from aqueous solutions: electron energy-loss spectroscopy, Auger spectroscopy, LEED, and cyclic voltammetry. *Langmuir* **1988**, *4*, 637–646.
- (12) Soriaga, M. P.; Hubbard, A. T. Determination of the orientation of adsorbed molecules at solid-liquid interfaces by thin-layer electrochemistry: aromatic compounds at platinum electrodes. *American Chemical Society* **1982**, *104*, 2735–2742.
- (13) Gattrell, M.; Kirk, D. W. A Study of the Oxidation of Phenol at Platinum and Preoxidized Platinum Surfaces. *J. Electrochem. Soc.* **1993**, *140*, 1534–1540.
- (14) Łukaszewski, M.; Soszko, M.; Czerwinski, A. Electrochemical Methods of Real Surface Area Determination of Noble Metal Electrodes – an Overview. *Int. J. Electrochem. Sci.* **2016**, 4442–4469.
- (15) Du, F.; Dao, T. A.; Peitl, P. V. J.; Bauer, A.; Preuss, K.; Bonastre, A. M.; Sharman, J.; Spikes, G.; Perchthaler, M.; Schmidt, T. J. *et al.* Effects of PEMFC Operational History under Dry/Wet Conditions on Additional Voltage Losses due to Ionomer Migration. *J. Electrochem. Soc.* **2020**, *167*, 144513.

- (16) Jomori, S.; Komatsubara, K.; Nonoyama, N.; Kato, M.; Yoshida, T. An Experimental Study of the Effects of Operational History on Activity Changes in a PEMFC // An Experimental Study of the Effects of Operational History on Activity Changes in a PEMFC. *J. Electrochem. Soc.* **2013**, *160*, F1067-F1073.
- (17) van Cleve, T.; Khandavalli, S.; Chowdhury, A.; Medina, S.; Pylypenko, S.; Wang, M.; More, K. L.; Kariuki, N.; Myers, D. J.; Weber, A. Z. *et al.* Dictating Pt-Based Electrocatalyst Performance in Polymer Electrolyte Fuel Cells, from Formulation to Application. *ACS applied materials & interfaces* **2019**, *11*, 46953–46964.
- (18) Kusoglu, A.; Weber, A. Z. New Insights into Perfluorinated Sulfonic-Acid Ionomers. *Chemical reviews* **2017**, *117*, 987–1104.
- (19) Yarlagadda, V.; Carpenter, M. K.; Moylan, T. E.; Kukreja, R. S.; Koestner, R.; Gu, W.; Thompson, L.; Kongkanand, A. Boosting Fuel Cell Performance with Accessible Carbon Mesopores. *ACS Energy Lett.* **2018**, *3*, 618–621.
- (20) Omata, T.; Uchida, M.; Uchida, H.; Watanabe, M.; Miyatake, K. Effect of platinum loading on fuel cell cathode performance using hydrocarbon ionomers as binders. *Physical chemistry chemical physics : PCCP* **2012**, *14*, 16713–16718.
- (21) U.S. Department of Energy. Fuel Cell Technical Team Roadmap. https://www.energy.gov/sites/prod/files/2017/11/f46/FCTT_Roadmap_Nov_2017_FINAL.pdf (accessed December 21, 2020).